A Statistical study of the Doppler spectral width of high-latitude ionospheric F-region echoes recorded with SuperDARN coherent HF radars

J.-P. Villain, R. André, M. Pinnock, R. A. Greenwald, C. Hanuise

Annales Geophysicae (2002) 20: 1769–1781 © European Geosciences Union 2002

Annales Geophysicae

A Statistical study of the Doppler spectral width of high-latitude ionospheric F-region echoes recorded with SuperDARN coherent HF radars

J.-P. Villain[1], **R. André**[1], **M. Pinnock**[2], **R. A. Greenwald**[3], **and C. Hanuise**[4,*]

[1]LPCE/CNRS, 3A Av. de la Recherche Scientifique, 45071 Orléans Cedex, France
[2]British Antarctic Survey, High Cross, Madingley Road, CB3 OET Cambridge, UK
[3]The Johns Hopkins University, Applied Physics Laboratory, Laurel, Maryland, USA
[4]LSEET/CNRS, Université de Toulon et du Var, BP 132, 83957 La Garde Cedex, France
[*]now at LPCE/CNRS

Received: 27 August 2001 – Revised: 13 June 2002 – Accepted: 17 June 2002

Abstract. The HF radars of the Super Dual Auroral Radar Network (SuperDARN) provide measurements of the $\boldsymbol{E} \times \boldsymbol{B}$ drift of ionospheric plasma over extended regions of the high-latitude ionosphere. We have conducted a statistical study of the associated Doppler spectral width of ionospheric F-region echoes. The study has been conducted with all available radars from the Northern Hemisphere for 2 specific periods of time. Period 1 corresponds to the winter months of 1994, while period 2 covers October 1996 to March 1997. The distributions of data points and average spectral width are presented as a function of Magnetic Latitude and Magnetic Local Time. The databases are very consistent and exhibit the same features. The most stringent features are: a region of very high spectral width, collocated with the ionospheric LLBL/cusp/mantle region; an oval shaped region of high spectral width, whose equatorward boundary matches the poleward limit of the Holzworth and Meng auroral oval. A simulation has been conducted to evaluate the geometrical and instrumental effects on the spectral width. It shows that these effects cannot account for the observed spectral features. It is then concluded that these specific spectral width characteristics are the signature of ionospheric/magnetospheric coupling phenomena.

Key words. Ionosphere (auroral ionosphere; ionosphere-magnetosphere interactions; ionospheric irregularities)

1 Introduction

Doppler spectra of ionospheric irregularities were initially obtained from E-region scatter with VHF radars in the early 60's (e.g. Bowles and Cohen, 1962). Coherent spectra give an estimation of the velocity distribution function of scattering irregularities present in the illuminated volume during the integration time. The first moment is related to the mean Doppler phase velocity of the irregularities in the scattering volume. In the absence of any large-scale spatial or temporal variations of the plasma velocity, the second moment, or spectral width, is representative of the turbulent motion induced by plasma instability mechanisms (microscale processes) causing the growth of the irregularities. Several types of irregularities have been identified (e.g. Fejer and Kelley, 1980).

In order to study the motion of ionospheric irregularities at HF wavelength a Doppler capability was introduced on classical ionosonde experiments (e.g. Bibl and Reinish, 1978). HF coherent radars were specifically designed to study ionospheric plasma processes and the first detailed auroral F-region Doppler spectra were published by Hanuise et al. (1981). It was shown at that time that the phase velocity of F-region irregularities was not limited to the ion acoustic speed, as was the case for E-region irregularities. Moreover, several experiments indicated that the irregularities were drifting at the $\boldsymbol{E} \times \boldsymbol{B}/\mathrm{B}^2$ velocity (Villain et al., 1985; Ruohoniemi et al., 1987). Unlike the case for E-region irregularities, no specific categories of F-region irregularities could be identified through either the Doppler velocity or their spectral width (Baker et al., 1988). With the development of the SuperDARN (Super Dual Auroral Radar Network) network (Greenwald et al., 1995), HF radars became one of the major tools to study ionospheric convection and ionosphere/magnetosphere coupling. In case studies, the spectral width has been used as a means to identify the ionospheric signature of magnetospheric regions or boundaries (e.g. Baker et al., 1986, 1995; Milan et al., 1999; Pinnock et al., 1995; Rodger et al., 1995). These authors have proposed several mechanisms to explain enhanced spectral width, such as larger than normal electric field turbulence (Baker et al., 1990; Rodger et al., 1995), structured precipitation (Dudeney et al., 1998) or Pc1 activity (André et al., 2000b).

Several statistical studies have been conducted with SuperDARN coherent HF radars. These studies concentrated mostly on backscatter occurrence (Ruohoniemi and Green-

Correspondence to: J.-P. Villain (jvillain@cnrs-orleans.fr)

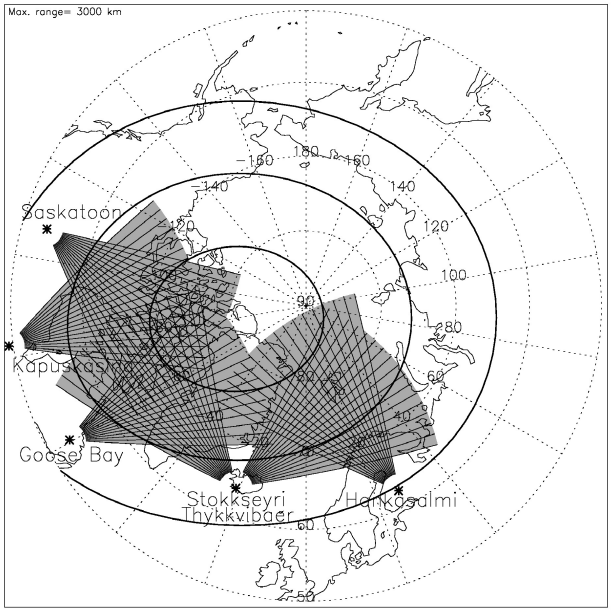

Fig. 1. Location and fields of view of the SuperDARN radars used in this study. The contours in thick lines correspond to the Invariant Latitudes of 60°, 70° and 80°.

wald, 1997; Milan et al., 1997) and on convection patterns (Ruohoniemi and Greenwald, 1996). As noted above, numerous studies have used spectral width in conjunction with low-altitude satellite measurements to map magnetospheric boundaries into the ionosphere, but no extensive study has been conducted to test the significance of the results on a statistical basis. Thus, in this paper, we present a statistical study of scatter location and spectral width using all available data from the Northern Hemisphere SuperDARN radars for two specific periods of time. Period 1 corresponds to the winter months of 1994, from January to March, with three radars in operation, and from September to December, with four radars in operation. Period 2 covers from October 1996 through March 1997, with six radars in operation.

The second objective of this paper is to evaluate the source of the spectral width parameters. In a realistic situation, the width can be affected by the finite size of the radar resolution cell and the length of the integration time. One has to take these and other sources of velocity variations into account when evaluating the spectral width. Velocity gradients present in the large-scale convection pattern are one potential source of spectral broadening.

In the following section, we describe the database and the results of our analysis. We then evaluate the contribution of the large-scale convection pattern to the spectral width. Finally, we discuss the relative influence of the different instrumental and geophysical sources on the spectral width. We conclude with a discussion on the ability of the SuperDARN HF radars to identify the signature of ionospheric-magnetospheric coupling phenomena and to monitor the projection of magnetospheric boundaries into the ionosphere.

2 Database and analysis

The algorithm to extract the spectral width from the multipulse autocorrelation function has been described by Villain et al. (1987). In the course of time, the data processing software has been modified, leading to a change in the value of the spectral width computed from some data sets. For each of the periods selected, care has been taken to ensure that the radars were running the same version of the fitting programs, so that each period is internally consistent. The first period corresponds to the months January to March and September to December of the year 1994. Three radars (Goose Bay, Kapuskasing and Saskatoon) were operated continuously during the year, and the Stokkseyri (Iceland West) radar started continuous operation at the end of August 1994. The second period spans 6 months of wintertime, starting from October 1996 until March 1997. The six radars of the Northern Hemisphere chain, in operation at that time, were used. It includes the four radars mentioned above as well as the Thykkvibær (Iceland East) and Hankasalmi (Finland) radars. The locations and fields-of-view of the radars are shown in Fig. 1. The comparison between these two periods allows us to check the consistency of the radar data over an extended period of time. There are three categories of radar operations, as described by Greenwald et al. (1995): Common Programs, Special Programs and Discretionary Operations. The Common Program consists of a basic scan repeated continuously, while the other modes allow for the radar to be operated differently. For our analysis only Common Program data have been selected.

2.1 The grid

The data are presented using a polar projection onto an MLT/Λ (Invariant Magnetic Latitude) grid with a $\frac{1}{2}$ h and one degree resolution using AACGM coordinates (Baker and Wing, 1989).

2.2 Selection criteria

For the selected periods and radars, each data record corresponds to an integration time of 6 or 7 s in each beam direction. The data are processed in the following way:

- Ground scatter returns are rejected using the criteria defined in Baker et al. (1988). These echoes are characterized by a simultaneous near-zero Doppler shift and spectral width.
- Echoes recorded at ranges less than 900 km are rejected to eliminate direct E-region echoes. At ranges greater than 900 km, E-region echoes may be observed through a one and a half hop mode of propagation, but their number is relatively small.
- At least three points, with two in consecutive range gates, to avoid spurious signal.
- Signal-to-noise ratios must be greater than 3 dB.

From the radar location, beam direction, range and UT, each selected point is then attributed to a given MLT-Λ grid point as defined above. The power is binned in 1 dB steps and the spectral width in 50 m/s steps.

2.3 Average IMF and K_p values

The average values of IMF and K_p have been computed for the statistical study. For period 1 the average K_p was 3^-, and the average values of the three IMF components were $B_x = 1.0\,\mathrm{nT}$, $B_y = -3.5\,\mathrm{nT}$ and $B_z = -1.2\,\mathrm{nT}$. For period 2, the average K_p was 2^+ , and the average values of the three IMF components were $B_x = 0.7\,\mathrm{nT}$, $B_y = -0.3\,\mathrm{nT}$ and $B_z = -0.3\,\mathrm{nT}$. The B_z values are rather small, but can be explained by the fact that for higher magnetic activity, the auroral oval and associated particle precipitation are displaced toward the radars or may even move equatorward of them. This can have two major effects: one is screening of the F-region by enhanced E-region ionisation; the other is absorption of the radar signals due to ionisation of the D-layer by very energetic particles. Both of these effects lead to more scatter during less disturbed periods. The IMF B_y values are significantly different for the two periods. Some effects attributed to this difference will be discussed.

2.4 Distribution of data points

The number of data points selected for each period is similar (14.6 10^6 and 13.9 10^6 for periods 1 and 2, respectively). The distributions of these data points are presented in Fig. 2a and b for periods 1 and 2, respectively. The two distributions are similar. The color bar indicates the number of points present in each MLT-Λ cell. The two color bars cover approximately the same ranges, with maximum values of 60 000 and 55 000 data points per cell for periods 1 and 2, respectively. The plots exhibit similar characteristics. Between 08:00 and 13:00 MLT and between 75° and 80° magnetic latitude, we observe in both figures a maximum in the number of data points. Period 2 exhibits its largest values just after 12:00 MLT. After 12:00 MLT, the maximum number of data points moves gradually toward lower latitudes at a rate of approximately one degree of latitude per half hour of MLT. This behaviour is similar for both periods. The enhancement reaches its lowest latitude of 68°, around 16:00 MLT. For period 1, the maximum number of data points is observed around 17:00 MLT at a latitude of 70°.

For the period of time from 12:00 to 16:00 MLT, the high-latitude boundary of the enhancement is located near 78° for period 1 and 80° for period 2. At 17:30 MLT, the distribution for period 2 narrows very rapidly to a band extending from 74° to 80° in latitude. In contrast, the distribution for period 1 remains very broad in latitude up to 22:00 MLT and is shifted to lower latitudes . After 22:00 MLT, for period 1 and 20:00 MLT for period 2, the distributions of data points become more latitudinally confined and decrease in amplitude. These changes are very smooth and end with a band of data points centered on 74° latitude. The minimum of points is observed for both periods between 04:00 and 07:00 MLT.

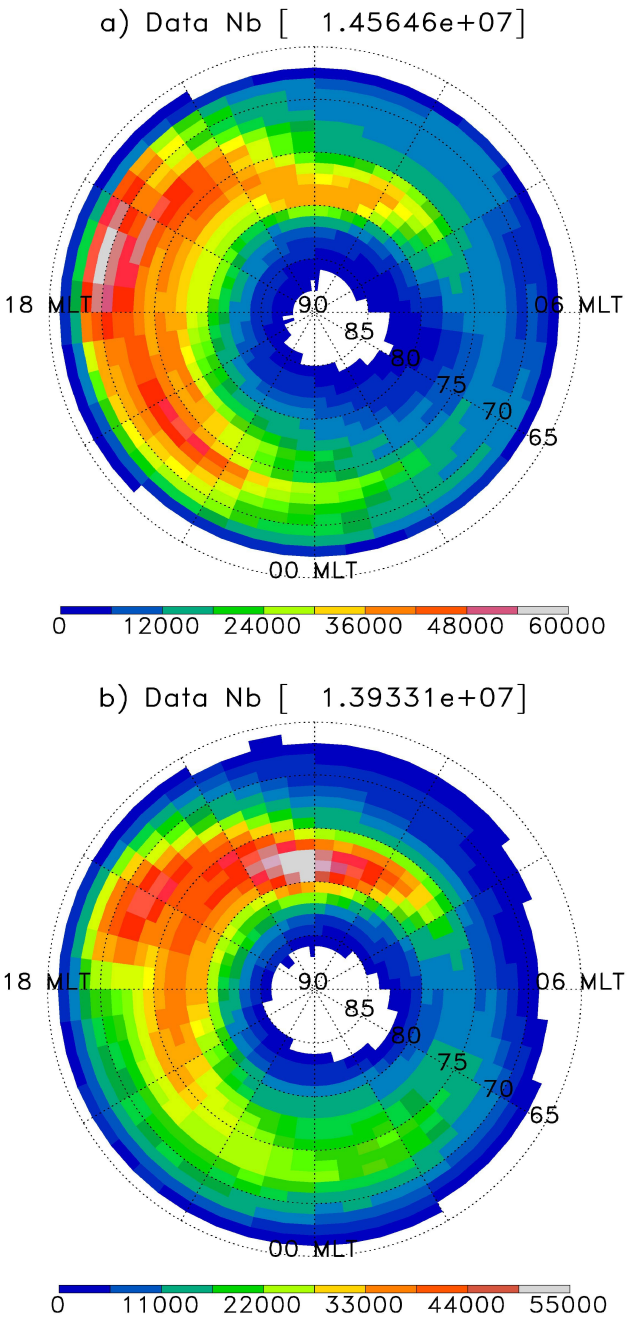

Fig. 2. Distribution of data points as a function of MLT and Magnetic Latitude for period 1 (Fig. 2a) and period 2 (Fig. 2b). The color scale indicates the number of points in each MLT-Λ cell.

Comparison of these two distributions shows consistency of the radar observations over very long periods of time, despite inherent variations of the geophysical conditions. The differences may be attributed to the locations and orientations of the additional radars that give access to regions not probed in period 1. There are also changes in the operating parameters of the radars during the latter period.

It is interesting to highlight the contribution of each radar to the database. This has been done for period 2 only. Figure 3 shows for each MLT-Λ cell the percentage of data points provided by each radar. It shows clearly that nightside scatter is obtained mainly by the Stokkseyri and Thykkvibær radars, both in Iceland. These radars are located at higher magnetic latitudes (around 65°), as shown on Fig. 1, and their orientation is more along the L-shell than the other radars. Their more poleward location implies that they are less affected by absorption or E-region screening due to energetic particle precipitation. On the dayside, nearly all radars contribute to the database. But some radars seem to have easier access to particular MLT-Λ regions. For example, the Kapuskasing radar makes the most important contribution in the early morning sector. One has to mention that during this period, the Goose Bay radar had a lower contribution due to some technical limitations.

As noticed previously, the radar orientation has a crucial impact on its ability to illuminate a given MLT-Λ region. For each radar and each MLT-Λ cell, a preferred beam number is defined as the average of the beam numbers associated to each and all data points. In the Northern Hemisphere, the beams are numbered from 0 to 15 in a clockwise direction. If one refers to Fig. 1, one can note that a given beam number does not correspond to the same orientation of the transmitting direction for different radars. Figure 4 displays the results of this analysis. The Stokkseyri and Thykkvibær radars exhibit a clear relation of magnetic latitude with beam number, as expected from their field of view orientation (see Fig. 1). For the four other radars, a very specific feature appears that has not been previously identified. These radars show a clear tendency to observe scatter preferentially with the low beam number in the morning sector and with a high beam number in the afternoon, regardless of their relative orientation. A detailed study of this feature is beyond the scope of this paper, but some interpretation can be proposed. This feature may be due to propagation/absorption effects caused by the levels of ionisation between the morning and afternoon sectors. Another more speculative interpretation can be given. If one considers a two-cell convection pattern, the preferred low beam numbers for the morning sector correspond to positive Doppler velocities and the high beam numbers for the afternoon sector also correspond to positive Doppler velocities. The observed feature would imply that the radars observe preferentially positive Doppler velocities. Such a feature has been observed for VHF radars on E-region irregularities by Mattin and Jones (1987) and interpreted theoretically by Janhunen (1994) in terms of plasma instability mechanisms. No similar study has yet been conducted on F-region irregularities.

2.5 Results

Figure 5 displays the results of the statistical study on the average spectral width for period 1 (Fig. 5a) and period 2 (Fig. 5b). The distributions of average spectral width are even more similar for both periods than the distributions of data points. One can see that the color scales are slightly different for the two periods (range 0 to 320 m/s and 0 to 400 m/s for periods 1 and 2, respectively). This is to compensate for the variations in spectral width due to the different versions of the fitting programs.

The main features of these plots can be described as follows. Both distributions exhibit an oval shaped region of enhanced spectral width extending towards lower latitudes in the midnight sector. The equatorward limit of this oval is rather sharp (transition from orange to green) and well defined. The location of this lower latitude boundary is the same within one degree at any MLT for both distributions. The noon side of the oval is characterized by a region of very high spectral width. This region extends from 76° to 81° in magnetic latitude and from 08:00 to 14:00 MLT. The region of high spectral width seems to be related to the cusp/cleft/mantle signature, referred to hereafter as the cusp. The spectral width signature of this region is rather extensive due to the movements in cusp location with solar wind parameters.

While this cusp signature is approximately centered around 12:00 MLT for period 1, it is displaced toward the morning side by more than one hour in MLT for period 2. By referring to the average IMF B_y conditions for these periods, one can note a marked difference in B_y with $B_y = -3.5$ for period 1, while $B_y = -0.3$ for period 2. Our observation of the spectral width of the cusp location and its shift in MLT with B_y is in agreement with previous statistical studies conducted on a high-latitude convection pattern. Ruohoniemi and Greenwald (1996), using SuperDARN data, found that, on average, the two-cell convection pattern is generally rotated from noon towards earlier MLTs and that for a negative B_y it is aligned with the noon-midnight meridian. Senior et al. (1990) present a statistical model of convection derived from incoherent scatter observations carried out with the EISCAT facility located in Scandinavia. They also reported a persistent rotation of the two-cell pattern toward earlier MLTs.

Above $\simeq 82°$, the spectral width decreases. This feature is well defined in period 2, but is less clear in period 1. The difference may be due to the somewhat lower number of data points in this latitude range for period 1.

Equatorward of the oval of enhanced spectral width, the distributions show smooth variations as a function of both latitude and MLT, but no specific feature. A more detailed analysis of spectral-width properties for period 2 is presented in Fig. 6. The upper left panel presents the distribution of the average power as a function of MLT-λ. The distribution of average power presents some similarities with the distribution of data points. These similarities are expected, since both distributions are affected by the same geophysical factors: propagation, radar-wave absorption and the presence of field-aligned irregularities. The distribution of power shows three regions with enhanced power: the cusp, the low-latitude afternoon sector and a band of backscatter centered around 75° in latitude and extending from 18:00 to 04:00 MLT on the nightside. It can be seen in Fig. 2b that

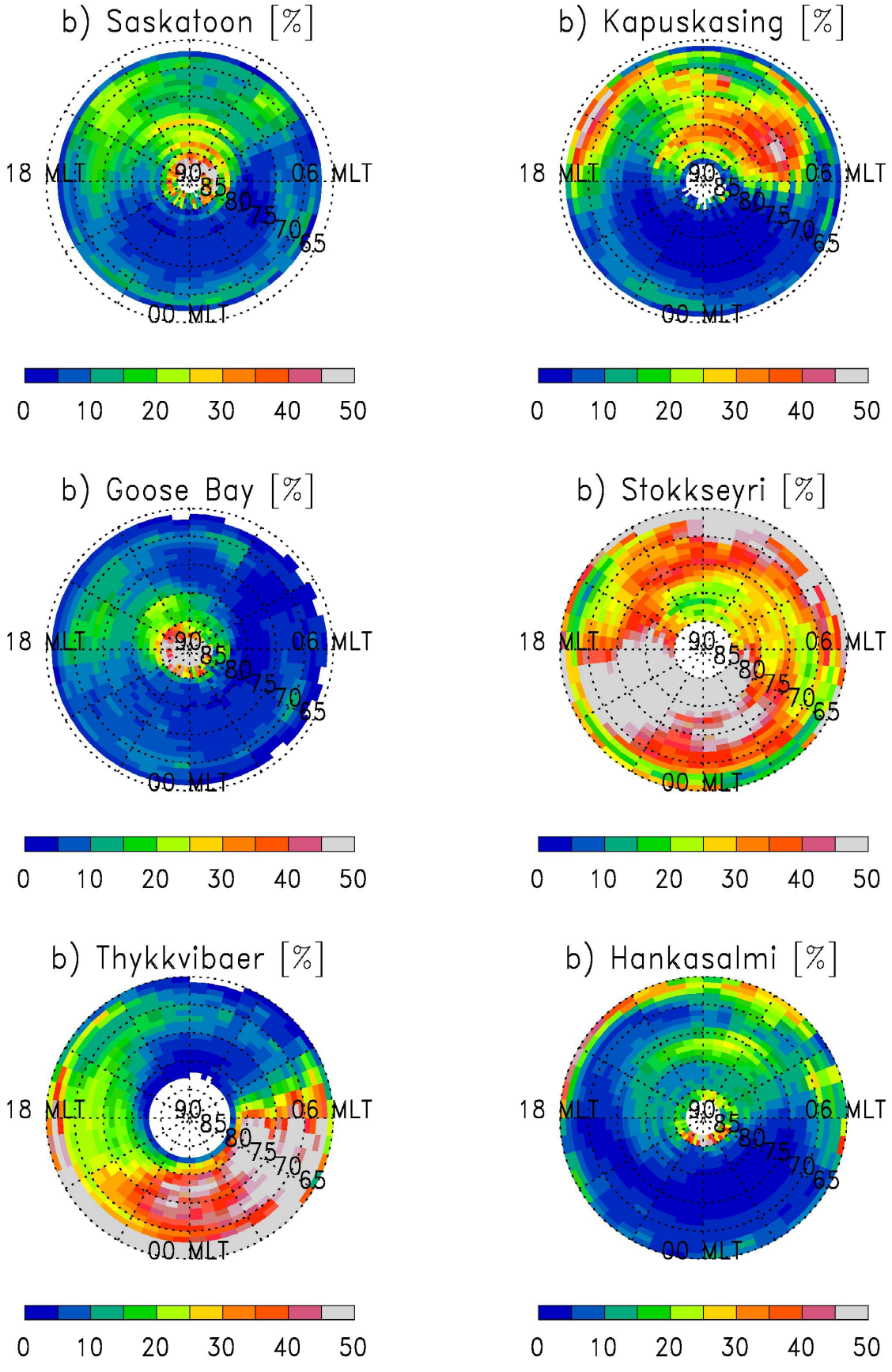

Fig. 3. Percentage of data points provided by each radar for each MLT-Λ cell for period 2.

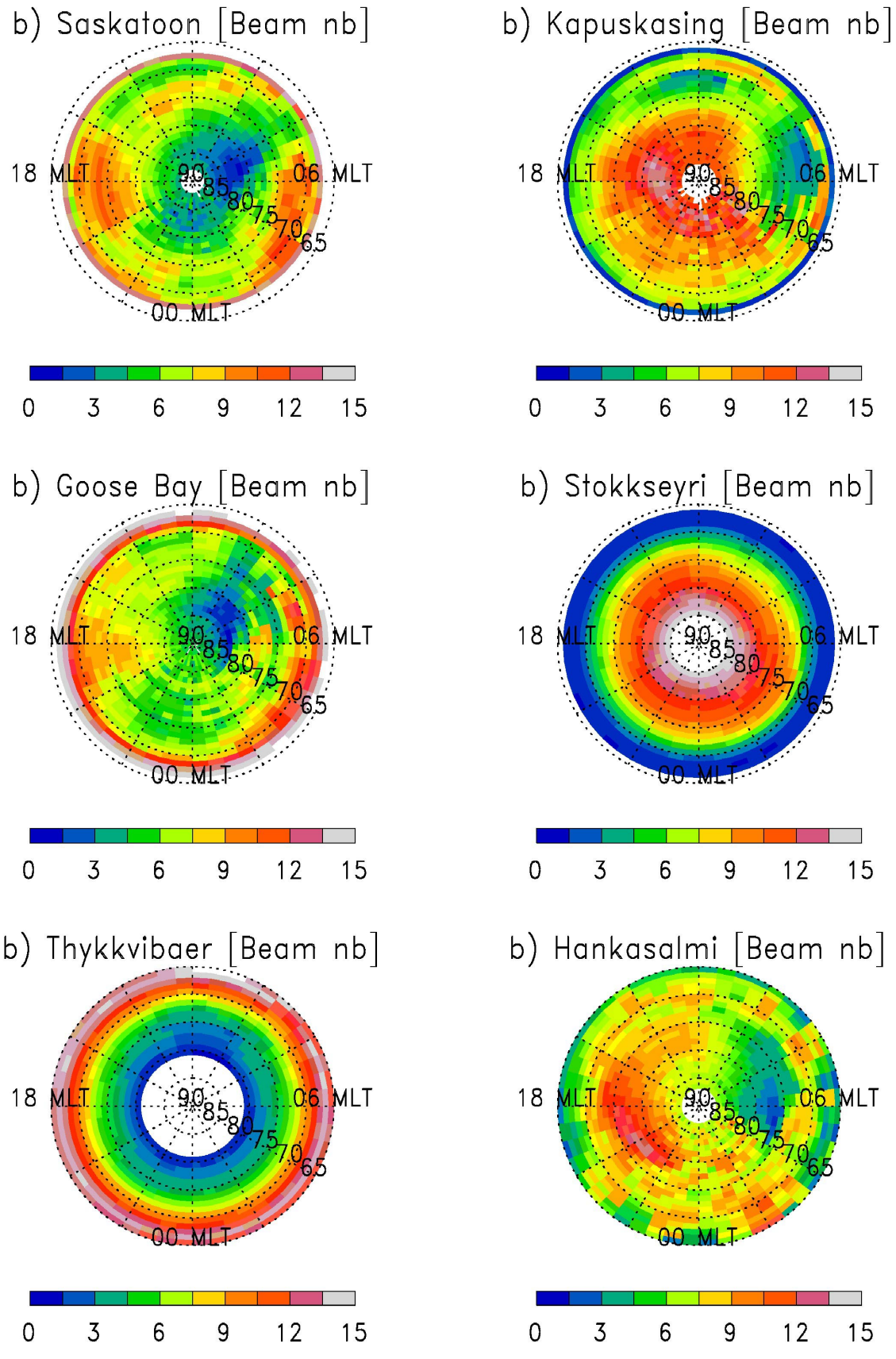

Fig. 4. Distribution of preferred beam number for each radar and each MLT-Λ cell for period 2. Beams are numbered from 0 to 15 in a clockwise direction. The fields of view are presented in Fig. 1.

the third region is not associated with a high number of data points.

It is important to note that the distribution of spectral width is totally independent of the distributions of data points and average power. The observed boundaries do not match each other, and the spectral width is not affected by the low number of data points and power observed in the 06:00 MLT sector.

The lower left panel of Fig. 6 again displays the spectral-width distribution for period 2, but with contours superimposed. The contour that is localized in the noon sector corresponds to the statistical location of the cusp region determined from low-altitude satellite data (Newell and Meng, 1988, 1992). This contour matches well with the region of very high spectral width, although the latter is extended toward somewhat earlier MLTs. It can be noted that the region corresponding to the Low Latitude Boundary Layer (LLBL), as observed from particle precipitation (Newell and Meng, 1992), is also shifted towards earlier MLT.

The second contour corresponds to the average position of the poleward boundary of the auroral oval, as modeled by Holzworth and Meng (1975) for moderate activity, which corresponds to the average K_p for this statistical study. It can be observed that apart from the cusp sector, this contour follows very closely the boundary between the high and low spectral width regions. On this plot, three white rectangles indicate cells for which histograms of the spectral width are presented in the lower right panel of Fig. 6. They are representative of the three regions defined from the spectral width characteristics. At low latitude in the afternoon sector, the histogram (plotted in black) is narrow, peaking at 100 m/s, with an average value of 192 m/s and with less than 5% of the spectral-width determinations greater than 300 m/s. In the region of enhanced spectral width in the night sector, the histogram (plotted in red) is wider, peaking at 200 m/s, with an average value of 250 m/s and with about 22% of the spectral-width determinations greater than 300 m/s. In the cusp, the histogram (plotted in blue) is even wider, peaking at 250 m/s, with an average value of 349 m/s due to its long tail, and with nearly 50% of the spectral-width determinations greater than 300 m/s. These histograms are representative of each region and are largely independent of their location within the region.

Finally, the upper right panel of Fig. 6 displays in the same reference frame the percentage of spectral-width determinations greater than 300 m/s for each MLT-Λ cell. The distribution of this parameter follows a pattern similar to the distribution of the average width. It is of the order of 50% in a well-defined band of latitude extending from 76° to 81° in latitude and from 04:00 to 13:00 MLT. Near noon, it is colocated with the cusp, but it also extends into the morning sector to 04:00 MLT.

The results of this analysis can be summarized as follows:

– The distributions of data points for two different periods of time, separated by more than two years and with different numbers of radars, show strong similarities. These features are controlled mainly by the same geophysical factors: propagation conditions, radar-wave absorption and the presence of field-aligned irregularities.

– The distributions of average power are similar to the distribution of data points. This is to be expected, since the backscatter power is also under the control of the same

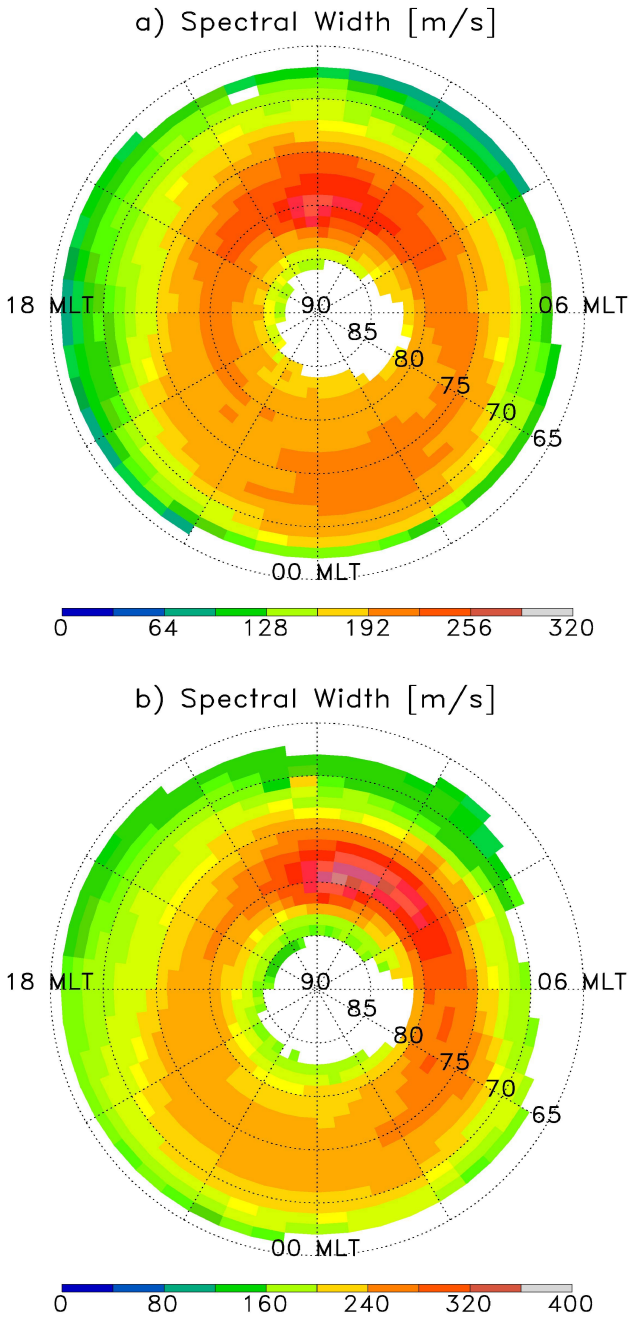

Fig. 5. Average spectral width as a function of MLT and Magnetic Latitude for period 1 (Fig. 5a) and period 2 (Fig. 5b). The color scales differ slightly in order to take into account the variation in spectral width due to the different versions of the fitting programs for the two periods.

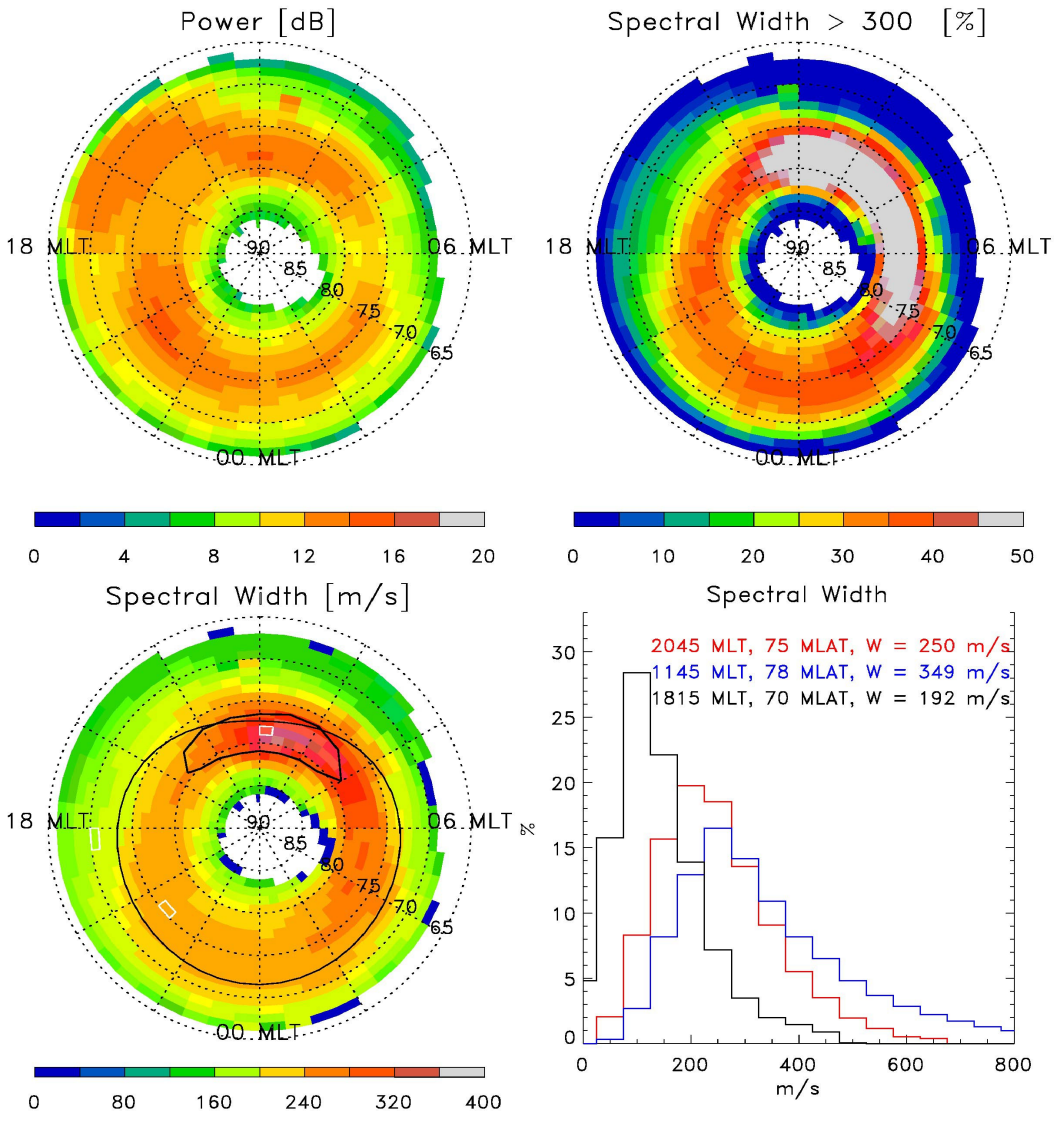

Fig. 6. Upper left corner: Distribution of average power in dB in the MLT-Λ reference frame. Lower left corner: Average spectral width in the MLT-Λ reference frame. The LLBL/cusp/mantle contour, defined by Newell and Meng (1992), and the poleward limit of the auroral oval for moderate magnetic activity, defined by Holzworth and Meng (1975), are superimposed. The three white rectangles indicate the location for which the histograms of spectral width are plotted in the lower right corner. Upper right corner: Percentage of spectral width greater than 300 m/s. Lower right corner: Histograms of spectral width and their average value for the three selected cells marked by white rectangles in the lower left plot.

geophysical parameters.

– The distribution of average spectral width has no relation with the previously discussed distributions. Three regions are clearly identified, whose boundaries are related to the footprint of well-defined magnetospheric regions.

3 Evaluation of geometrical effects on the spectral width

The second part of the paper now examines geometrical and instrumental characteristics that can affect the determination of the spectral width. The large-scale convection pattern introduces horizontal velocity gradients in the radar cells that increase the width of the velocity distribution. A simulation has been conducted to evaluate these geometrical effects on the spectral width. It makes use of the Heppner and Maynard (1987) empirical convection model for average K_p conditions and takes into account the particular characteristics of each radar (location, beam directions, size and orientation of each radar cell). In the vertical direction, ray-tracing studies (e.g. André et al., 1997) have shown that the scattering region is localized close to the maximum of the F-region electron density. At high-latitude, the Earth's magnetic field lines are nearly vertical and considered as equipotential. The

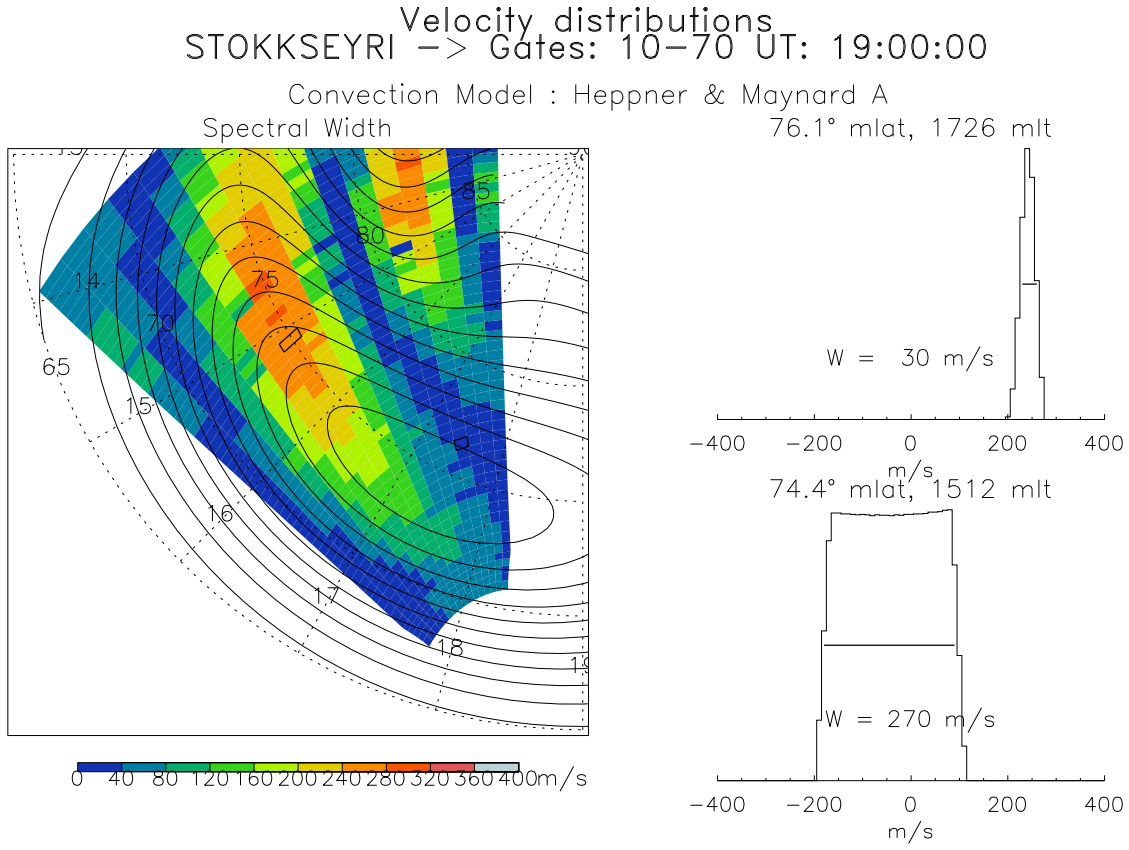

Fig. 7. Spectral width enhancement introduced by an inhomogeneous plasma flow in a cell. Left: results of a simulation using the Heppner and Maynard convection model for the Stokkseyri radar for an instantaneous scan in an MLT-λ reference frame. Right: Spectral width for two particular cells indicated in the left plot by small black rectangles located, respectively, at 76.1° MLAT and 17:26 MLT in a region of homogeneous plasma flow and at 74.4° MLAT and 15:12 MLT in a region of velocity reversal.

radars are only sensitive to irregularities moving perpendicular to the magnetic field, and there is no vertical gradient of the horizontal velocity within the scattering volume. Therefore, there is no vertical velocity variation in the scattering volume.

3.1 Methodology

The signal observed by the radar is obtained through Bragg scattering by ionospheric irregularities having a scale length of half the radar wavelength. These irregularities are created through plasma instability mechanisms, such as the gradient drift instability (e.g. Keskinen and Ossakow, 1983) producing a turbulent medium. In an homogeneous ionosphere with no variation of the geophysical parameters in the radar cell, the observed spectral width is representative of the turbulence produced by the considered instability mechanism. In this section, in order to describe this effect, we use the term “turbulence scattering the radar-wave”.

The spectral width inherent to the turbulence scattering the radar-wave is set to zero and only the macroscale component due to the plasma flow velocity variations in a cell is considered. One has to evaluate the width of this velocity distribution function recorded by each radar for each range gate as a function of Universal Time (UT). The radar cells are divided into subcells, defining a spatial resolution of 1 km in both radial and azimuthal directions. This corresponds to approximately 4500 subcells for a cell at a range of 1500 km from the radar. We assume uniform backscattered power from each of these subcells. Then, for a given beam and range gate at a particular time, one can compute the radial velocity in each subcell from the Heppner and Maynard convection model. Thus, we are able to compute in each cell the radial velocity distribution function and to extract its width. An example of such a computation is shown in Fig. 7. The left panel displays the computed spectral width for the Stokkseyri radar field of view at 19:00 UT (the radar is probing the afternoon convection cell). Isocontours of the electric potential defined by the Heppner and Maynard model are superimposed. The right-hand panels of Fig. 7 show the radial velocity distribution function for two individual cells identified in the left panel by black contours. The distribution function displayed in the upper right-hand panel has been computed in a region of homogeneous flow (73.1 MLAT, 17:26 MLT), and exhibits a width of only 30 m/s. This value is much smaller than the width inherent to the turbulence scattering the radar-wave usually observed (100–200 m/s) (Hanuise et al., 1993).

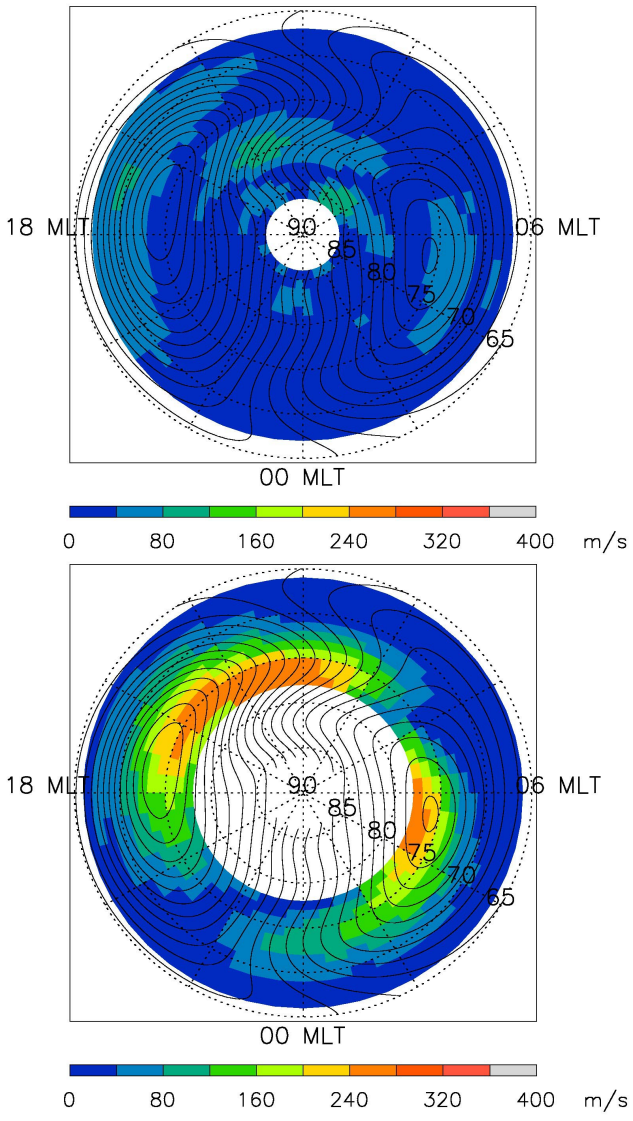

Fig. 8. Beam orientation effect on spectral width enhancement introduced by inhomogeneous plasma flow in a cell. Top: MLT-Λ plot for beam 4 of the Goose Bay radar. Bottom: MLT-Λ plot for beam 12 of the Goose Bay radar.

The distribution function displayed in the lower right-hand panel has been computed in the velocity convection reversal at 74.4 MLAT and 15:02 MLT. The spectral width is much higher (270 m/s) and is of the same order of magnitude as the width induced by the turbulence scattering the radar-wave. In the left panel of Fig. 7, one can observe that the effect of the large-scale plasma convection on the spectral width can be of the same order as the inherent width, due to the turbulence scattering the radar-wave in a region of sharp radial velocity gradient.

The beam direction has a crucial influence on this estimated spectral width. Figure 8 displays this parameter averaged over UT in the MLT-Λ grid for beam 12 (nearly aligned along L-shell) and beam 4 (along a magnetic meridian) of the Goose Bay radar on the left and right panels, respectively.

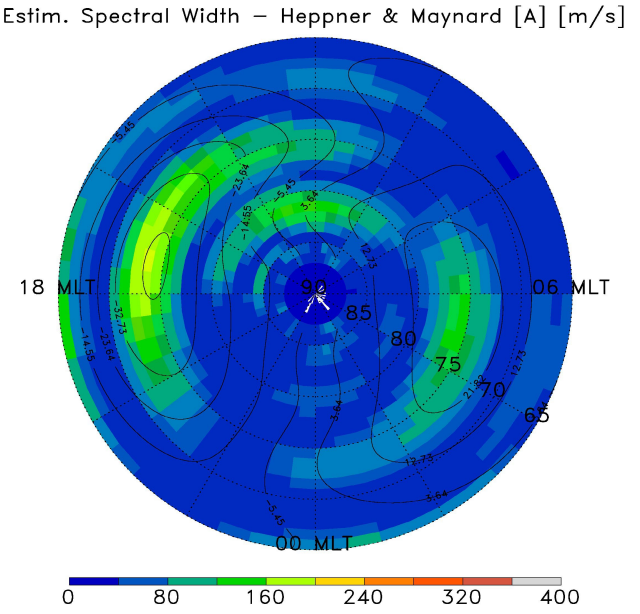

Fig. 9. Distribution of simulated MLT-Λ spectral width enhancement introduced by plasma convection corresponding to the whole database of period 2 using the Heppner and Maynard convection model for a K_p of 2^+.

The spectral width recorded by beam 12 is higher only inside the convection reversals, whereas the width recorded by beam 4 is always very small, except at very high-latitudes. For example, at 77 MLAT and 16:00 MLT, the value of the width introduced by the finite size of the radar cell is greater than 200 m/s when recorded by beam 12 and lower than 50 m/s when recorded by beam 4.

Finally, one can estimate the contribution of the large-scale convection pattern to the spectral width distribution observed from our database. For each measurement included in the statistical study, one has computed the contribution to the spectral width due to the variations of the plasma convection velocity in the cell corresponding to the given radar, given beam direction and range. The distribution over MLT-Λ is displayed on Fig. 9. Again, the estimated spectral width is higher (around 200 m/s on average) in regions that correspond to convection reversals, and very small (around 50 m/s) elsewhere. If one compares these results with the observed average spectral width (lower left-hand panel of Fig. 6), it clearly does not account for the observed spectral width distribution.

To summarise the geometrical and instrumental effects on spectral width induced by the large-scale convection pattern, one can observe that there is no direct evidence of such an effect on the distribution of spectral width. These geometrical effects certainly produce spectral width enhancement for specific convection patterns and at specific times, but they cannot explain the observed distribution in spectral width.

4 Discussion

The distribution of average spectral width as a function of MLT-Λ presents well-defined regions, whose boundaries can be related with the footprint of magnetospheric regions. The distribution of data points may depend on radar location, beam orientation and other phenomena related to propagation, absorption, or the presence of field-aligned irregularities. But when data are obtained, the observed spectral width seems clearly associated with ionospheric/magnetospheric coupling phenomena. We will now discuss for each of the identified regions the possible coupling mechanism involved with the spectral width signature observed in the HF radar Doppler spectra.

4.1 Cusp identification

One of the most stringent features in this statistical study is the region of very high spectral width located between 76° and 80° of magnetic latitude and centered around 11:00 MLT. It is also clearly visible with the large enhancement in the data point distribution for both periods involved in this study. This feature is collocated with the LLBL/cusp/mantle average position as given by Newell and Meng (1992), using the DMSP low-altitude spacecraft. Moreover, this quantity is very high ($>$ 350 m/s) in a region that corresponds to the cusp. Baker et al. (1990, 1995) have found a clear association of this high spectral width region with the cusp defined by low-altitude satellites. This correlation has been used to evaluate the reconnection rate across this boundary (Baker et al., 1997; Pinnock et al., 1999). André et al. (1999, 2000b) have explained these large spectral width values by the low-frequency wave activity (Pc1) recorded on board satellites (Maynard et al., 1991; Matsuoka et al., 1993; Erlandson and Anderson, 1996). Electric field variations in the Pc1 frequency band are not resolved by radars, but integrated in such a way that they introduce several unreal components in the Doppler spectrum due to aliasing (André et al., 2000a). The routine analysis method used cannot discriminate multi-component spectra and leads to the determination of a very high spectral width.

4.2 Oval boundary

The second feature that can be clearly seen in the spectral width distribution in Fig. 5 is the oval shaped region of high spectral width (250 m/s). The lower boundary of this region reaches its lowest magnetic latitude of 72° in the midnight sector. In Fig. 6, it was shown that it could be associated with the average position of the poleward boundary of the auroral oval (Holzworth and Meng, 1975; Feldstein and Starkov, 1967) for moderate activity. In a statistical study, such as this one, this contour cannot be taken as an absolute boundary, but rather as an indication that the region under consideration could be linked to the footprint of the magnetic field lines originating in the outermost regions of the magnetosphere. In fact, Dudeney et al. (1998) have investigated the spectral width behaviour in the midnight sector during a conjunction with the POLAR satellite. They have found a sharp latitudinal increase of the spectral width collocated with the boundary between the Central Plasma Sheet (CPS) and the Boundary Plasma Sheet (BPS), where the electron precipitations become more structured and the intensity of electrostatic waves below 100 Hz increased.

4.3 Lower latitudes

The spectral width is lower (around 150 m/s) equatorwards of this limit. This region may correspond to the footprint of closed field lines, not associated with the outermost regions of the magnetosphere, and on which the phenomena driving the spectral width enhancement are different. For example, higher energy electron fluxes associated with visual auroras are depositing their energy in the E-region rather than the F-region and may have less influence on the spectral width.

4.4 Very high-latitudes

Finally, it was observed that the spectral width decreases at very high-latitudes. This region is the footprint of open field lines connected directly with the Interplanetary Magnetic Field (IMF). In general, these field lines are less affected by any kind of energy deposition, from particle precipitation or wave activity.

4.5 Early morning sector

4.5.1 Radar-wave absorption

Another feature that appears clearly in the database is the absence of scatter for almost any latitude in the 06:00 MLT sector. This feature was already mentioned by Ruohoniemi and Greenwald (1997) in a statistical study of backscatter from the Goose Bay HF radar alone. This lack of data could be attributed to radar-wave absorption. Precipitation of very energetic electrons in this region is causing D-region ionisation (Foppiano and Bradley, 1985). This enhanced D-region ionisation is able to cause absorption of the radar-wave, especially in the HF band, strongly decreasing the signal-to-noise ratio of the radar and thus, the number of data points. However, when data are available, the Doppler spectral width seems to be well defined and rather high.

4.5.2 High spectral width

The presence of such high spectral width in this MLT sector is not yet fully understood. The combination of very low ionospheric electron density (end of night during wintertime), combined with the structured precipitation mentioned above, could induce such an increase in the spectral width. This feature needs to be investigated.

5 Conclusion

In this study we have created a large database of SuperDARN radar echo characteristics (power and spectral width) using data from two different periods separated by 2 years. We have found that their characteristics and main features are very similar, showing the consistency of the radar observations over a long period of time. One has evaluated by simulation the contribution of the large-scale electric field convection pattern to the spectral width due to experimental characteristics (finite cell size, radar location and orientation). We have shown that the radial velocity gradient could contribute to the spectral width, but, on average, the observed distribution of spectral width is not affected by these large-scale effects. The features observed in the MLT/Λ distribution of the spectral width, even if they could not be related unambiguously to specific regions of the magnetosphere, could be shown to be the signature of ionospheric-magnetospheric coupling phenomena:

- A region of very high spectral width (350 m/s) is collocated with the ionospheric cusp/cleft region.
- An oval shaped region of high spectral width (250 m/s) near the poleward limit of the Holzworth and Meng auroral oval. This region could be linked to magnetic field lines originating in the outermost regions of the magnetosphere.
- A region of lower spectral width at lower latitude that could be related to closed field lines, associated with regions located deeper in the magnetosphere.
- A region of lower spectral width at very high-latitudes that could be related to magnetic field lines connected with the Interplanetary Magnetic Field (IMF).
- A region of reduced radar backscatter in the 06:00 MLT sector is attributed to structured energetic electron precipitation causing radar-wave absorption and enhanced spectral width.

Acknowledgement. The operation of the SuperDARN radars in the Northern Hemisphere used in this study is supported by the national funding agencies of the U. S., Canada, the U. K., and France.

Topical Editor M. Lester thanks M. L. Parkinson and C. Lathuillère for their help in evaluating this paper.

References

André, R., Hanuise, C., Villain, J.-P., and Cerisier, J.-C.; HF radars: Multi-frequency study of refraction effects and localization of scattering, Radio Sci., 32, 153–168, 1997.

André, R., Pinnock, M., and Rodger, A. S.: On the SuperDARN autocorrelation function observed in the cusp, Geophys. Res. Lett., 26, 3353–3356, 1999.

André, R., Pinnock, M., and Rodger, A. S.: Identification of the low altitude cusp by SuperDARN radars: A physical explanation for the emperically derived signature, J. Geophys. Res., 105, 27 081–27 093, 2000a.

André, R., Pinnock, M., Rodger, A. S., Villain, J.-P., and Hanuise, C.: On the factors conditioning the Doppler spectral width determined from SuperDARN HF radars, Int. J. Geomag. Aeron., 2, 77–86, 2000b.

Baker, K. B. and Wing, S.: A new magnetic coordinate system for conjugate studies at high-latitudes, J. Geophys. Res., 94, 9139–9147, 1989.

Baker, K. B., Greenwald, R. A., Walker, A. D. M., Bythrow, P. F., Zanetti, L. J., Potemra, T. A., Hardy, D. A., Rich, F. J., and Rino, C. L.: A case study of plasma processes in the dayside cleft, J. Geophys. Res., 91, 3130–3144, 1986.

Baker, K. B., Greenwald, R. A., Villain, J.-P., and Wing, S.: Spectral characteristics of high frequency (HF) backscatter from high-latitude ionospheric irregularities : Preliminary analysis of statistical properties, Tech. Rep. RADC-TR-87-204, Rome Air Development Center, Griffis Air Force Base, NY, 1988.

Baker, K. B., Greenwald, R. A., Ruohoniemi, J. M., Dudeney, J. R., Pinnock, M., Newell, P. T., Greenspan, M. E., and Meng, C.-I.: Simultaneous HF-radar and DMSP observations of the cusp, Geophys. Res. Lett., 17, 1869–1872, 1990.

Baker, K. B., Dudeney, J. R., Greenwald, R. A., Pinnock, M., Newell, P., Rodger, A. S., Mattin, N., and Meng, C.-I.: HF-radar signatures of the cusp and low-latitude boundary layer, J. Geophys. Res., 100, 7671–7695, 1995.

Baker, K. B., Rodger, A. S., and Lu, G.: HF-radar observations of the dayside magnetic merging rate: A Geospace Environment Modeling boundary layer campaign study, J. Geophys. Res., 102, 9603–9617, 1997.

Bibl, K. and Reinish, B. W.: The universal digital ionosonde, Radio Sci., 13, 519–530, 1978.

Bowles, K. L. and Cohen, E.: A study of radio wave scattering from sporadic E near the magnetic equator, in Ionospheric sporadic E, (Eds) Smith, E. and Matsushita, S., Pergammon Press, New York, 1962.

Dudeney, J. R., Rodger, A. S., Freeman, M. P., Pickett, J., Scudder, J., Sofko, G. J., and Lester, M.: The nightside ionospheric response to IMF By changes, Geophys. Res. Lett., 25, 2601–2604, 1998.

Erlandson, R. E. and Anderson, B. J.: Pc1 waves in the ionosphere: A statistical study, J. Geophys. Res., 101, 7843–7857, 1996.

Fejer, B. G. and Kelley, M. C.: Ionospheric irregularities, Rev. Geophys. Space Phys., 18, 401–454, 1980.

Feldstein, Y. I. and Starkov, G. V.: Dynamics of auroral belt and polar geomagnetic disturbances, Planet. Space Sci., 15, 209–229, 1967.

Foppiano, A. J. and Bradley, P. A.: Morphology of background auroral absorption, J. Atmos. Terr. Phys., 47, 663–674, 1985.

Greenwald, R. A., Baker, K. B., Dudeney, J. R., Pinnock, M., Jones, T. B., Thomas, E. C., Villain, J.-P., Cerisier, J.-C., Senior, C., Hanuise, C., Hunsucker, R. D., Sofko, G. J., Koehler, J., Nielsen, E., Pellinen, R., Walker, A. D. M., Sato, N., and Yamagishi, H.: DARN/SuperDARN: A global view of the dynamics of high-latitude convection, Space Sci. Rev., 71, 761–796, 1995.

Hanuise, C., Villain, J.-P., and Crochet, M.: Spectral studies of *F*-region irregularities in the auroral zone, Geophys. Res. Lett., 8, 1033–1036, 1981.

Hanuise, C., Villain, J.-P., Grésillon, D., Cabrit, B., Greenwald, R. A., and Baker, K. B.: Interpretation of HF-radar Doppler spectra by collective wave scattering theory, Ann. Geophysicae, 11, 29–39, 1993.

Heppner, J. P. and Maynard, N. C.: Empirical high-latitude electric field models, J. Geophys. Res., 92, 4467–4489, 1987.

Holzworth, R. H. and Meng, C.-I.: Mathematical representation of the auroral oval, Geophys. Res. Lett., 2, 377, 1975.

Janhunen, P.: Perpendicular particle simulation of the *E*-region Farley-Buneman instability, J. Geophys. Res., 99, 11 461–11 473, 1994.

Keskinen, M. J. and Ossakow, S. L.: Non linear evolution of convective plasma enhancements in the auroral ionosphere, 2. Small scale irregularities, J. Geophys. Res., 88, 474–482, 1983.

Matsuoka, A., Tsuruda, K., Hayakawa, H., Mukai, T., Nishida, A., Okada, T., Kaya, N., and Fukunishi, H.: Electric field fluctuations and charged particle precipitation in the cusp, J. Geophys. Res., 98, 11 225–11 234, 1993.

Mattin, N. and Jones, T. B.: Propagation angle dependance of radar auroral *E*-region irregularities, J. Atmos. Terr. Phys., 49, 115–121, 1987.

Maynard, N. C., Aggson, T. L., Basinka, E. M., Burke, W., Craven, P., Peterson, W. K., Sugiura, M., and Weimer, D. R.: Magnetospheric boundary dynamics : DE1 and DE2 observations near the magnetopause and cusp, J. Geophys. Res., 96, 3505–3522, 1991.

Milan, S. E., Yeoman, T. K., Lester, M., Thomas, E. C., and Jones, T. B.: Initial backscatter occurence statistics from the CUTLASS HF radars, Ann. Geophysicae, 15, 703–718, 1997.

Milan, S. E., Lester, M., Cowley, S. W. H., Moen, J., Sandholt, P. E., and Owen, C. J.: Meridian-scanning photometer, coherent HF radar, and magnetometer observations of the cusp: a case study, Ann. Geophysicae, 17, 159–172, 1999.

Newell, P. T. and Meng, C.-I.: The cusp and the cleft/boundary layer: Low-altitude identification and statistical local time variation, J. Geophys. Res., 93, 14 549–14 556, 1988.

Newell, P. T. and Meng, C.-I.: Mapping the dayside ionosphere to the magnetosphere according to particle precipitation characteristics, Geophys. Res. Lett., 19, 609–612, 1992.

Pinnock, M., Rodger, A. S., Dudeney, J. R., Rich, F., and Baker, K. B.: High-spatial and temporal observations of the ionospheric cusp, Ann. Geophysicae, 13, 919–925, 1995.

Pinnock, M., Rodger, A. S., Baker, K. B., Lu, G., and Hairston, M.: Conjugate observations of the day-side reconnection electric field: A GEM boundary layer campaign, Ann. Geophysicae, 17, 443–454, 1999.

Rodger, A. S., Mende, S. B., Rosenberg, T. J., and Baker, K. B.: Simultaneous optical and HF radar observations of the ionospheric cusp, Geophys. Res. Lett., 22, 2045–2048, 1995.

Ruohoniemi, J. M. and Greenwald, R. A.: Statistical patterns of high-latitude convection obtained from Goose Bay HF radar observations, J. Geophys. Res., 101, 21 743–21 763, 1996.

Ruohoniemi, J. M. and Greenwald, R. A.: Rates of scattering occurence in routine HF radar observations during solar cycle maximum, Radio Sci., 32, 1051–1070, 1997.

Ruohoniemi, J. M., Greenwald, R. A., Baker, K. B., Villain, J.-P., and McCready, M. A.: Drift motions of small scale irregularities in the high-latitude F region: An experimental comparison with plasma drift motions, J. Geophys. Res., 92, 4553–4564, 1987.

Senior, C., Fontaine, D., Caudal, G., Alcaydé, D., and Fontanari, J.: Convection electric fields and electrostatic potential over $61^\circ < \lambda < 72^\circ$ invariant latitude observed with the European incoherent scatter facility, 2, Statistical results, Ann. Geophysicae, 8, 257–272, 1990.

Villain, J.-P., Caudal, G., and Hanuise, C.: A SAFARI-EISCAT comparison between the velocity of *F*-region small scale irregularities and the ion drift, J. Geophys. Res., 90, 8433–8443, 1985.

Villain, J.-P., Greenwald, R. A., Baker, K. B., and Ruohoniemi, J. M.: HF radar observations of *E*-region plasma irregularities produced by oblique electron streaming, J. Geophys. Res., 92, 12 327–12 342, 1987.